Autonomous Thrust-Assisted Perching of a Fixed-Wing UAV on Vertical Surfaces

Dino Mehanovic(✉), John Bass, Thomas Courteau, David Rancourt, and Alexis Lussier Desbiens

Université de Sherbrooke, Sherbrooke, QC J1K 2R1, Canada
{dino.mehanovic,alexis.lussier.desbiens}@usherbrooke.ca
http://www.createk.design

Abstract. We present the first fixed-wing drone that autonomously perches and takes off from vertical surfaces. Inspired by birds, this airplane uses a thrust-assisted pitch-up maneuver to slow down rapidly before touchdown. Microspines are used to cling to rough walls, while strictly onboard sensing is used for control. The effect of thrust on the suspension's landing envelope is analyzed and a simple vertical velocity controller is proposed to create smooth and robust descents towards a wall. Multiple landings are performed over a range of flight conditions (a video of S-MAD is available at: http://createk.recherche.usherbrooke.ca/LM2017/).

Keywords: Perching · Multimodal · Scansorial · Fixed-wing · UAV · Drone · Bioinspired

1 Introduction

The increasing demand for civil applications of unmanned aerial vehicles (UAV) is encouraging the development of small platforms with extended mission life. However, small airframes have low aerodynamic efficiency and reduced energy storage capabilities, both of which severely limit the endurance and range of these platforms. In nature, many small birds, insects and mammals regularly land to rest, feed, seek shelter or stealthily monitor an area.

Recently, a variety of bioinspired robotic platforms have been created for perching and are reviewed in detail in [1]. Among those, quadrotors have been used due to their ability to perform agile flight trajectories to slow down before impact [2,3]. Directly flying into targets has also been explored by appropriately positioning adhesives on fixed-wing and multi-rotor airframes [4–7]. To perform both perching and climbing on vertical surfaces, the SCAMP quadrotor re-orients itself after flying directly into a wall [8].

The implementation of such perching capabilities in a powered fixed-wing UAV remains a challenge for various reasons (e.g., added mass by propulsion system). Thus, the most successful solutions are based on glider platforms unable to take off [9–11]. Notably, the perching trajectory for the Stanford Perching

M. Mangan et al. (Eds.): Living Machines 2017, LNAI 10384, pp. 302–314, 2017.
DOI: 10.1007/978-3-319-63537-8_26

Fig. 1. Many birds exhibit landing trajectories with high body pitch angles and significant upward force to maintain a horizontal approach. Courtesy of: Maxis Gamez (a), PCO (b), Warren Photography (c) and Kaddy (d).

Glider is inspired by the flying squirrel [11]. It performs a pitch-up maneuver followed by a drag-affected ballistic phase, before adhering to vertical surfaces with microspines. However, the ballistic phase creates only a short zone of suitable touchdown conditions that impose severe requirements on the platform's wall sensor, as discussed further in Sect. 2.

Sherbrooke's Multimodal Autonomous Drone (S-MAD), presented in this paper, draws inspiration from nature in order to perform full cycles of landing, standby, takeoff and flight (LSTF). As illustrated in Fig. 1, many birds use high body pitch angles and significant upward force to maintain horizontal perching approaches. This paper demonstrates that such a thrust-assisted landing strategy, when utilized on a fixed-wing aircraft, enables controlled steady-state descents (SSD) towards perching sites. This reduces the impact speed and significantly extends the zone of suitable touchdown conditions, leading to enhanced reliability and reduced hardware requirements (e.g., suspension, wall sensing). This landing strategy also enables simple takeoff, facilitated by the favorable thrust orientation while perched. To our knowledge, this is the first autonomous fixed-wing platform capable of performing both perching and takeoff maneuvers.

2 Perching Strategy Overview

The thrust-assisted perching maneuver described in this paper builds onto previous work that enabled a fixed-wing glider to perch on vertical surfaces following a rapid feedforward pitch-up maneuver [12]. This maneuver, illustrated by the dotted line in Fig. 2, rapidly slows down the glider and exposes the landing gear to the vertical surface. As the glider reaches full pitch-up, the velocity is reduced to such an extent that aerodynamic forces become negligible and the glider keeps travelling on a mostly ballistic trajectory towards the wall. With proper timing, the airplane touches down with a sufficiently low speed to allow a suspension to dissipate the remaining kinetic energy, while favoring the feet attachment to the surface. This approach leads to high success rates on airframes with low wing loading, even with the use of a simple feedforward controller [11]. However,

increasing the mass of the platform with additional payload and motors causes the suspension touchdown envelope (i.e., the set of touchdown states that lead to successful landing) to shrink down to negligible size. At the same time, the increased wing loading makes it more challenging to reduce the forward velocity to acceptable levels, before gravity significantly increases the vertical velocity to unacceptable values. Thus, as the mass increases, fewer trajectories can bring the glider from normal flying conditions to the suspension's touchdown envelope, leading to reduced success rate.

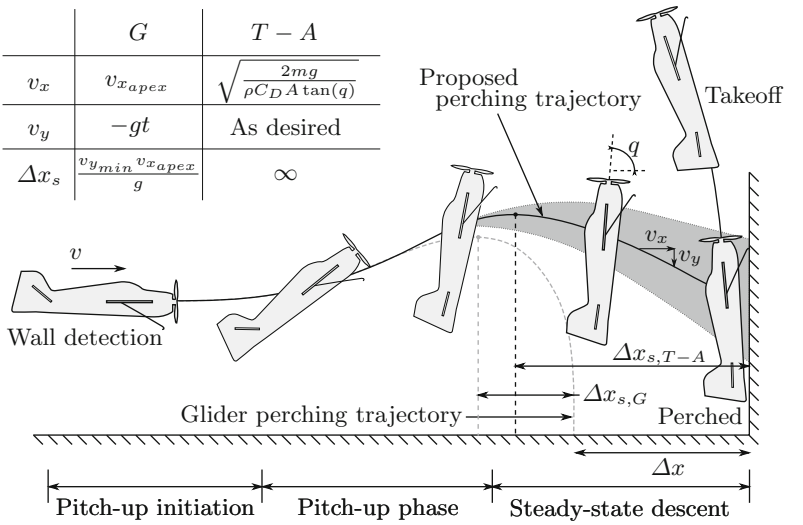

Fig. 2. Representation of the proposed thrust-assisted ($T-A$) perching strategy and comparison to a glider (G) trajectory. Variations in SSD's velocity slope, e.g., induced by sensor bias or battery level, are represented by the shaded area. Post-apex velocities and Δx_s shown in the top-left table, where g is the gravitational acceleration and t is time. Allowable wall detection error gain for $T-A$ over G is identified by Δx.

Comparatively, the approach described in this paper takes advantage of thrust to control the final vertical and forward velocities such that:

1. Suitable touchdown conditions are available during an extended distance to reduce the timing and sensing requirement needed to trigger the maneuver.
2. Lower impact speeds are experienced by the suspension, leading to size and mass reduction.
3. Approach trajectories that favor adhesive engagement can be used.
4. Control authority is maintained throughout the full maneuver due to the propeller flow on the control surfaces. This allows early termination of the perching maneuver and recovery until the final stages of the maneuver.
5. Takeoff is possible, enabling repeated cycles of LSTF during a single mission.

The final approach of both gliding and thrust-assisted trajectories can easily be compared conceptually from the apex conditions (i.e., $v_x = v_{x_{apex}}$, $v_y = 0$), by assuming limits on the allowable velocity at landing (i.e., $0 < v_x < v_{x_{max}}$ and $v_{y_{min}} < v_y < 0$). In the case of the glider, velocity as a function of time and distance travelled while maintaining suitable touchdown states (Δx_s) can be calculated by assuming a ballistic trajectory, as expressed in Fig. 2. Comparatively, the post-apex steady-state trajectory of the thrust-assisted maneuver can be described by assuming a constant pitch (q), and by equating the vertical thrust component to mg and the horizontal component to the drag ($1/2\rho C_D A v_x^2$). Velocities and distance travelled while maintaining suitable touchdown states are described in Fig. 2.

As expected, thrust-assisted perching allows the designer to specify the velocity at touchdown given (1) the physical parameters mg/A, (2) the commanded pitch approach angle (q) and (3) assuming that v_y can be measured and controlled through thrust. Under these conditions, the airplane can travel an indefinite distance in states suitable for touchdown. This is an important gain over the gliding maneuver, for which the Δx_s distance is on the order of 20 cm and thus imposes strict sensing requirements.

However, the addition of thrust also adds some challenges. Indeed, any remaining thrust at impact (e.g., propeller spin down after touchdown detection through onboard accelerometer) significantly modifies the touchdown envelope by reducing the shear forces experienced by the microspines and the corresponding adhesion. Thrust-assisted landing is also highly sensitive to numerous airframe parameters and initial flight conditions, reducing the success rate achievable by a simple feedforward maneuver. The following sections describe the implementation of thrust-assisted perching, analyze the effect of thrust on the touchdown envelope and propose a novel simple feedback controller based on vertical velocity.

3 Implementation

The airframe used in the experiments described in this paper is presented in Fig. 3. It consists of a modified McFoamy airplane (i.e., 12 A ESC, Turnigy 2730 1500 kV motor and 8×6 propeller for a static thrust-to-weight ratio of 1.5), combined with a 3DR PixHawk autopilot for onboard control. This autopilot integrates most required sensors required for vertical velocity estimation and impact detection (gyro, accelerometers, barometer), and communicates with a lightweight laser rangefinder (TeraRanger One) for wall detection. Custom control loops run onboard the PixHawk at 200 Hz.

Five microspines are used on each foot to attach onto vertical surfaces. Although various adhesion strategies exist [13], microspines are preferred due to their proven performance on numerous rough surfaces of interest (e.g., stucco, concrete, brick, roofing shingles) [14]. Inspired by insect feet, the microspines (Fig. 3) consist of hooks that attach to rough vertical surfaces through mechanical interference and friction, while distributing the load uniformly between asperities. As illustrated in Fig. 3, the microspines require shear and normal force

loadings within a safe zone delimited by friction, adhesion and overload limits to remain attached to the surface.

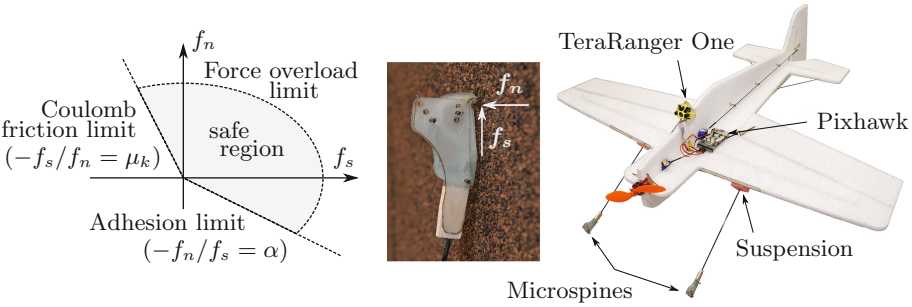

Fig. 3. Safe force region, microspines and platform components.

A suspension is installed between the airplane and the microspines to help bring the platform to rest, while favoring attachment to the surface. The suspension requirements for a thrust-assisted perching airplane are simplified due to the low touchdown speeds and the controlled touchdown direction. The proposed perching mechanism consists of a flexible beam, anchored in the airframe's wing and damped by a urethane foam block. At 18 g, the resulting suspension is significantly simpler and lighter than the suspension of the Stanford Perching Glider (28 g). Overall, with the added mass of the TeraRanger (15 g), the components required to enable perching only account for 10% of the platform's total mass (320 g).

4 Thrust-Assisted Touchdown Envelope

As discussed previously, the remaining thrust force during landing affects the touchdown envelope by reducing the shear force exerted at the feet and, incidentally, the adhesion available. This section describes the model developed to analyze the landing forces, its validation and the resulting landing envelope when thrust is present.

4.1 Model Description

The thrust-assisted perching maneuver described in this paper consists of mostly sagittal motion, with complex behaviors of the microspines at the feet. To properly represent this system, a hybrid planar dynamic model of the airplane and suspension is used, with both sliding and sticking states possible at the feet. By calculating the forces created during landing, and verifying if either the adhesion or the overload limit is reached, this model can predict the success or failure of different landing conditions.

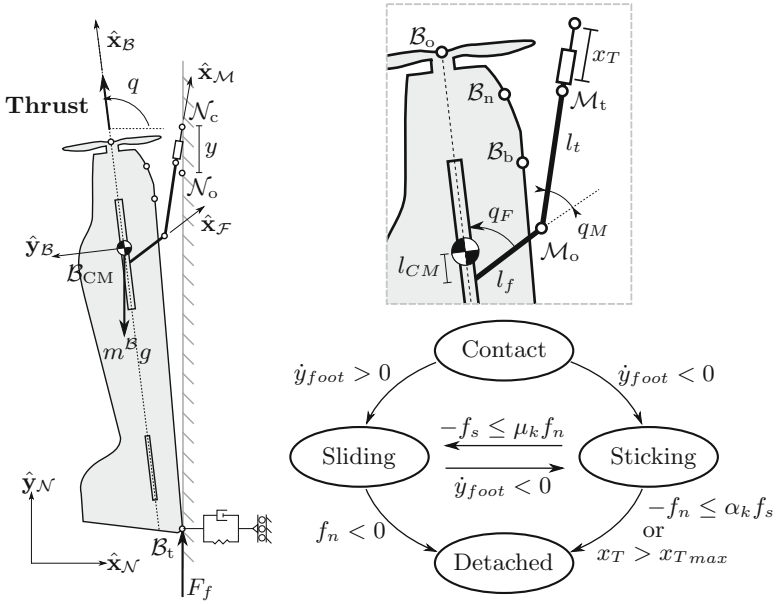

Fig. 4. System geometry, reference frames, forces and model transitions.

Figure 4 illustrates the geometry and forces defining the system, as well as the hybrid model states and discrete events leading to transitions. Besides the new suspension and added thrust, the model structure and contact dynamics at nose, belly and tail are similar to [11]. The airplane is modeled as a rigid body $\mathcal{B}$ and the legs are described by a single leg and foot. The combination of the leg's flexible beam and memory foam is modeled as a pseudo-rigid body [15], where two rigid segments (i.e., the fixed femur, $\mathcal{F}$, and the moving tibia $\mathcal{M}$) are connected by a pivot (knee) with lumped torsional stiffness and damping parameters. The foot is approximated by a linear spring-damper system. The thrust force is defined as a constant value ($m^{\mathcal{B}}g$) until impact detection (i.e., $14\,\mathrm{m/s^2}$ acceleration at CG). From that point, it follows an exponential decrease with an experimentally validated time constant of 85 ms. Due to the relatively low impact speed, the aerodynamic forces are neglected in this model. The contact point model at the foot can either take the form of a rolling joint (sliding) or a pin joint (sticking), depending on force and motion conditions at the foot, as described in the lower right transition diagram in Fig. 4.

Furthermore, as shown in Fig. 4, various reference frames and variables are introduced for the analysis. Without going into the details, it is easy to express the position of the airplane's center of mass ($\mathcal{B}_{\mathrm{CM}}$) as:

$$\mathbf{r}^{\mathcal{B}_{\mathrm{CM}}/\mathcal{N}_o} = y\hat{\mathbf{y}}_{\mathcal{N}} - (x_T + l_t)\hat{\mathbf{x}}_{\mathcal{M}} - l_f\hat{\mathbf{x}}_{\mathcal{F}} + l_{CM}\hat{\mathbf{x}}_{\mathcal{B}} \tag{1}$$

This vector, and other easily expressed quantities, can be used to establish the equations of motion through Kane's method for each generalized speed u_r [16].

The sliding foot model uses $\dot{q}$, $\dot{q}_M$ and $\dot{y}$ as generalized speeds (i.e., x_T is constant), while the sticking foot model uses $\dot{q}$, $\dot{q}_M$ and $\dot{x}_T$.

4.2 Model Validation

To confirm that the proposed model can accurately represent a wide range of touchdown conditions, four landings were performed by hand throwing the airplane without thrust on an instrumented force plate. Representative touchdown speeds of 1–2 m/s were used in various directions, as illustrated in Fig. 6, resulting in different loading trajectories that excite the full system dynamics. During these tests, constant pitch ($q = 86 \pm 3°$) and angular velocity ($\dot{q} = -50 \pm 30°/\text{s}$) were maintained, similar to the commanded states at touchdown.

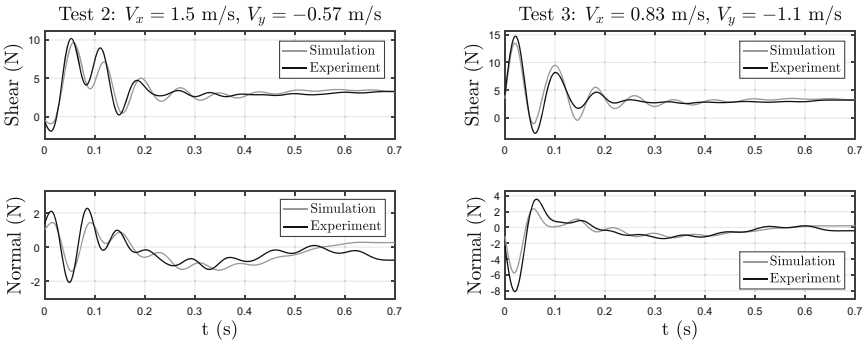

Fig. 5. Shear (f_s) and normal (f_n) forces acting on microspines at landing as obtained from simulations and experiments for tests 2 (left) and 3 (right).

The experimental setup used to measure shear and normal forces consists of a fabric-covered plate. This surface is used to guarantee simultaneous engagement of all microspines with the surface. The plate is instrumented using an ATI Mini40 force/torque sensor sampled at 1 kHz. The plate has a resonance frequency of at least 150 Hz in all directions. The recorded data is post-filtered using a 20 Hz Butterworth filter (20th order, zero-phase) to remove the structural modes of the airframe. The touchdown states are measured at 200 Hz using a motion capture system. Figure 5 shows the results for two tests.

Some physical parameters of the model were identified from the measured forces with a genetic algorithm (GA). To do so, the GA varies the selected physical parameters over a predefined range, aiming at minimizing the first 0.4 seconds of the normalized RMS (NRMS) error for shear and normal force in all four tests. The RMS error of each landing is normalized by its maximum absolute force range to produce a representative fit over different impact conditions. Each generation contains 100 individuals and the GA stops after the NRMS change over 5 generations is less than 0.01%. This condition was reached

Table 1. Physical properties of the system

Parameter	Symbol	Value	Source
Mass	$m^{\mathcal{B}}$	0.32 kg	Measured
Inertia	I_{zz}	0.017 kg m^2	GA
Pseudo-rigid body factor	γ	0.93	GA
Leg length	L	0.317 m	Measured
Femur and tibia length	l_f, l_t	0.022 m, 0.295 m	$(1-\gamma)L$, γL
Knee stiffness and damping	k_k, c_k	1.26 Nm/rad, 0.057 Nms/rad	GA
Foot stiffness and damping	k_f, c_f	2120 N/m, 5.32 Ns/m	GA
Wall stiffness and damping	k_w, c_w	231 N/m, 73 Ns/m	GA
Femur angle from fuselage	q_F	$-30°$	Measured
Spines natural length	l_0	0.0036 m	Measured

after 12 generations, with the NRMS error for all tests being less than 0.5%. The best parameters found with the GA are listed in Table 1.

The suspension's physical parameters obtained with the GA correspond to expected results: the inertia is slightly higher than our CAD model while the foot stiffness/damping are comparable to the results presented in [11]. The wall stiffness value is also significantly lower due to the softer nature of the EPP foam used on this airplane.

4.3 Landing State Map (LSM)

The calibrated model can be used to identify the envelope of impact states that lead to successful perching, as shown in Fig. 6. The LSM itself is validated with landings on a wall covered with asphalt shingles (i.e., $f_n/f_s < 1$). The platform is hand-thrown at various velocities, with angular speed and pitch angle maintained relatively constant. A total of 35 trials were performed as illustrated in Fig. 6, including six failures outside of the predicted success area. Slow-motion footage confirmed that these failures occurred through microspines overload, as predicted by the model.

This model can further be used to predict successful perching conditions when thrust is still present following touchdown (right LSM in Fig. 6). This LSM was calculated by considering the variable delay introduced by detecting the foot impact with the accelerometer located on the airplane's body, given the soft suspension, and by considering the motor spin-down. These effects significantly reduce and reshape the LSM's area (e.g., zone A in Fig. 6).

5 Perching Controller Design

The proposed pitch-up trajectory takes advantage of the airframe's high thrust-to-weight ratio to significantly extend the suitable horizontal distance available

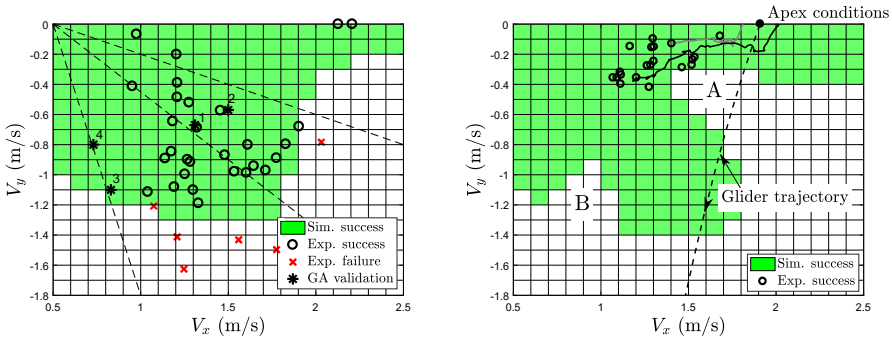

Fig. 6. Simulated LSM in green, with (right) and without (left) thrust. Simulations are performed with 5 spines engaged. (left) Experimental landings validating the simulated LSM ($q = 86 \pm 3°$, $\dot{q} = -50 \pm 30°/s$). Similar shear and normal force patterns are created for loading trajectories along the same radial dashed line. This reduces the number of necessary GA validation points for model calibration. (right) Touchdown velocity of 20 thrust-assisted approaches from horizontal flight. Two approach trajectories are also illustrated. (Color figure online)

for perching. However, thrust creates disturbances not present on a glider. These include yaw perturbation due to gyroscopic effect during pitch-up and roll perturbation, caused by the rotor torque required to accelerate the propeller at the entry of the SSD phase. To compensate for these perturbations, three decoupled PD feedback loops are used for each control surface [12,17]. Thrust-assisted perching is also difficult to perform under a feedforward control architecture. Indeed, small variations in initial battery voltage, airplane mass, CG position and launch speed all lead to large variations in the touchdown velocity and, consequently, failure to land as detailed in Table 2. The remainder of this section details a simple thrust controller, compares the results with feedforward control and describes tuning of the controller through the use of a classifier.

5.1 Thrust Control over Vertical Velocity (TCV^2)

To create the desired SSD phase favoring smooth landings under a wide range of conditions, the proposed thrust controller (TCV^2) utilizes a proportional feedback loop over RPM to maintain a desired vertical speed from wall detection. This feedback term is added to a constant command ($T_o \simeq mg$) as follows:

$$T_c = K_p(V_d - V_m) + T_o \tag{2}$$

where T_c is the output thrust, K_p is a proportional gain, V_d is the desired vertical speed, V_m is the measured vertical speed and T_o is the constant thrust command. The vertical speed is calculated through integration of the acceleration, starting from the Pixhawk estimate during horizontal flight.

Simulations are used to compare the TCV^2 and feedforward controller robustness by individually varying a set of nine variables that include airframe, actuator

and sensing parameters, along with initial condition variations (fixed wall detection distance of 5.5 m). To capture the dynamics of the complete perching maneuver, this study combines a flight dynamics model developed by Khan et al. [18] with the hybrid perching model described in Sect. 4. The selected flight dynamics model captures various important aspects of the proposed perching maneuver, e.g., unsteady and high-alpha aerodynamics, effects of control surface deflections and propeller slipstream effects.

Table 2. Varied parameters and success range for each controller (FR: Full range)

Parameter	Units	Baseline	Range	Feedforward	TCV^2
V_x (body-fixed frame)	m/s	8	[6; 10]	[7.1; 8.6]	FR
V_z (body-fixed frame)	m/s	0	[−2; 2]	FR	FR
Pitch	°	0	[−20; 20]	[−16.8; 20]	FR
Mass	kg	0.32	[0.28; 0.36]	[0.31; 0.34]	FR
Inertia	kg m2	0.017	[0.012; 0.012]	FR	FR
Angular Velocity	°/s	0	[−57; 57]	FR	FR
Range sensor error	m	0	[−0.3; 0.3]	[−0.3; 0.26]	FR
CG position*	cm	−31.3	[−33.3; −29.3]	[−31.3; −29.6]	[−31.3; −29.9]
Battery level	%	100	[80; 100]	[96; 100]	FR
Accelerometer bias	m/s^2	0	[−0.1; 0.1]	-	FR

* Distance taken from the airplane's nose.

The results, presented in Table 2, demonstrate the advantages of TCV^2 over a feedforward controller. The most sensible parameters for a feedforward controller are mass and battery level. If these parameters are not carefully tuned, the thrust and gravity forces are unbalanced and the vertical velocity varies throughout the maneuver. Changing the CG position also modifies the capability of the airplane to rapidly pitch-up, thus affecting the distance required to perform the maneuver. As expected, the TCV^2 feedback controller compensates for variations of almost all of these parameters.

5.2 TCV^2 Proportional Gain Sizing

A more thorough analysis is required to tune the controller for maximum success rate, given simultaneous variations of the identified parameters over their allowable range (Table 2). To speed up the analysis, a support vector machine (SVM) classifier that evaluates the combinations for successful landing is trained on the complete numerical model, which includes the aircraft's dynamics during flight and after impact with the wall. This classifier is trained using 30,000 simulations designed using a Latin hypercube sampling method. A set of 85% of these simulations is used for training and 15% for validation. Defining the SVM's Gaussian radial basis function kernel with $\sigma = 1.4$ in the normalized space, a prediction accuracy of 92.8% is achieved for the validation set. The success rate is evaluated for each K_p, assuming a uniform distribution of other parameters over their respective range.

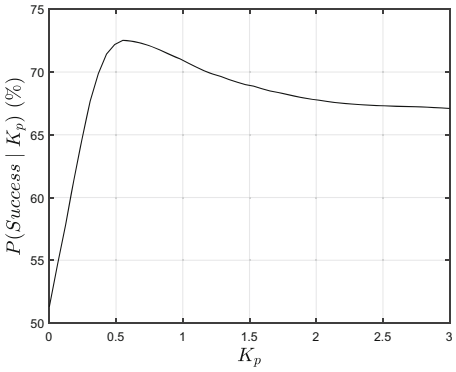

Fig. 7. Success probability of the perching maneuver for a known K_p.

The results of this analysis, shown in Fig. 7, reveal that a K_p value of approximately 0.5 leads to the highest probability of successful perching for the parameter variations described in Table 2. This probability rapidly decreases for lower K_p. A small proportional gain also introduces considerable increases in altitude - up to 6 m, as full thrust is applied throughout the full maneuver. Similarly, increasing the K_p value leads to excessively low thrust commands during the pitch-up phase which slows down the transition to SSD. This decreases the probability of success given a fixed wall detection distance.

6 Experimental Results

A series of tests were conducted on the platform presented previously. The airplane was launched towards a vertical wall covered with asphalt shingles at speeds ranging from 6.7 to 7.7 m/s. A total of 20 consecutive launches were performed, for which a 100% success rate was achieved. The touchdown velocities of these tests are mapped on the LSM (right) in Fig. 6, with two trajectories showing that the airplane maintains vertical descent speeds around the commanded value (−0.2 m/s). A typical landing is illustrated in Fig. 8. After such landing, the airplane can use its thrust to take off vertically as described in [12].

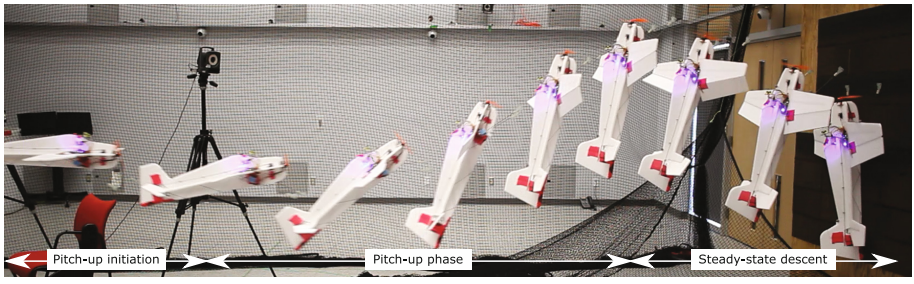

Fig. 8. Sequence of the thrust-assisted perching maneuver.

7 Conclusion and Future Work

This paper introduces S-MAD, the first fixed-wing UAV capable of thrust-assisted perching and takeoff. This small aerobatic platform performs a pitch up maneuver to rapidly slow down and expose its landing gear to vertical surfaces. A PixHawk controller samples the onboard sensors, including a laser range finder, and executes custom control loops to perform the maneuver autonomously.

Future work includes various improvements on the system, such as a more precise estimation of the vertical velocity and a mass reduction of the suspension. An important enhancement will also be the inclusion of non-contact sensors to turn off the propeller pre-emptively by early detection of incoming touchdowns. In the longer term, it is expected that this configuration of actuators, electronics and sensors will allow thrust-assisted wall climbing, aborted approaches and recovery from failed attachment.

The ability to perch reliably on vertical surfaces opens the door for repeated cycles of landing, standby, takeoff and flight. This enables extended mission durations for small UAVs, offering new types of applications. Ultimately, such bird-inspired platforms could be used for long duration surveillance, energy harvesting, inspection of structures or reconfigurable sensor networks.

Acknowledgement. This work was supported financially by FRQNT. We would like to thank the members of Createk and Prof. Nahon's lab at McGill for the great help that they provided throughout the realization of the work presented.

References

1. Roderick, W.R., Cutkosky, M.R., Lentink, D.: Touchdown to take-off: at the interface of flight and surface locomotion. Interface Focus **7**(1), 20160094 (2017)
2. Thomas, J., et al.: Aggressive flight with quadrotors for perching on inclined surfaces. J. Mech. Robot. **8**(5), 051007 (2016)
3. Myeong, W., et al.: Development of a drone-type wall-sticking and climbing robot. In: International Conference on Ubiquitous Robots and Ambient Intelligence (2015)
4. Kalantari, A., et al.: Autonomous perching and take-off on vertical walls for a quadrotor micro air vehicle. In: International Conference on Robotics and Automation (2015)
5. Liu, Y., Sun, G., Chen, H.: Impedance control of a bio-inspired flying and adhesion robot. In: International Conference on Robotics and Automation (2014)
6. Daler, L., et al.: A perching mechanism for flying robots using a fibre-based adhesive. In: International Conference on Robotics and Automation (2013)
7. Graule, M., et al.: Perching and takeoff of a robotic insect on overhangs using switchable electrostatic adhesion. Science **352**, 978–982 (2016)
8. Pope, M., et al.: A multimodal robot for perching and climbing on vertical outdoor surfaces. IEEE Trans. Robot. **33**, 38–48 (2016)
9. Moore, J., Cory, R., Tedrake, R.: Robust post-stall perching with a simple fixed-wing glider using LQR-trees. Bioinspir. Biomim. **9**(2), 025013 (2014)
10. Kovač, M., Germann, J., Hürzeler, C., Siegwart, R.Y., Floreano, D.: A perching mechanism for micro aerial vehicles. J. Micro-Nano Mech. **5**, 77–91 (2009)

11. Lussier Desbiens, A.: Landing and perching on vertical surfaces. Ph.D. thesis, Stanford University (2012)
12. Lussier Desbiens, A., Asbeck, A.T., Cutkosky, M.R.: Landing, perching and taking off from vertical surfaces. Int. J. Robot. Res. **30**, 355–370 (2011)
13. Schmidt, D., Berns, K.: Climbing robots for maintenance and inspections of vertical structures'a survey of design aspects and technologies. Robot. Auton. Syst. **61**(12), 1288–1305 (2013)
14. Asbeck, A., et al.: Scaling hard vertical surfaces with compliant microspine arrays. Int. J. Robot. Res. **25**, 1165–1179 (2006)
15. Howell, L.L.: Compliant Mechanisms. Wiley, New York (2001)
16. Mitiguy, P.: Advanced dynamics and motion simulation (2014)
17. Green, W.E., Oh, P.Y.: A hybrid mav for ingress and egress of urban environments. IEEE Trans. Robot. **25**, 253–263 (2009)
18. Khan, W., Nahon, M.: Modeling dynamics of agile fixed-wing UAVs for real-time applications. In: International Conference on Unmanned Aircraft Systems (2016)